The Investigation of Gaussian Beams and Optical Vortices Diffraction in the Near Zone of Subwavelength Optical Elements with Variable Height

Dmitry A. Savelyev[*]
Samara National Research University
Samara, Russian Federation

Abstract. The finite difference time domain method was used to simulate the propagation of Gaussian beams and optical vortices with circular, radial, azimuthal polarization on subwavelength ring gratings with standard and GRIN substrates in this paper. The height of individual zones of the optical elements relief was varied. It was shown that it is possible to select the beam type and element parameters in such a way that a long light needle (up to 8.2λ) and a narrow focal spot are formed on the optical axis (up to 0.33λ).

Keywords: Gaussian beams, optical vortices, FDTD, GRIN, subwavelength ring gratings, Meep.

Introduction

The materials and media with gradient refractive index (GRIN) have found wide application in many areas of human activity [1–13]. The use of GRIN materials for light collimation [8, 14], solving optical communication problems [15], light propagation control [5, 16], and in biology [6, 12] is well known. One of the main features of gradient refractive index media is the non-uniform distribution of the refractive index in space [2, 4, 9, 17]. Such media can be classified depending on the shape of the surfaces, for which the refractive index is constant [9], often distinguishing symmetrical GRIN media with respect to a given coordinate [9] and arbitrary GRIN media (F-GRIN), where an arbitrary three-dimensional distribution of the refractive index is observed [4]. Also, neural networks are known to be used for designing such media [18].

The vortex and Gaussian beams have been actively used to solve problems in optics and photonics [19–36] in recent years. In particular, such laser beams are used for tight focusing [16, 30, 25, 37], optical information transmission [22, 38], optical manipulation [20, 24, 35, 39–41], and probing [42]. To generate such beams, it is known to use such optical structures as metalenses and metasurfaces [8, 20, 43], spiral phase plates [20, 44, 45], and ring gratings [46–48]. It should be noted that ring gratings and diffraction axicons in various combinations are also used to obtain optical needles with a large focal depth [30, 34, 49–51].

The diffraction of Laguerre–Gaussian modes $(0,0)$ and $(0,1)$ (Gaussian beams and first-order optical vortices with the azimuthal index is equal to one were considered) with circular, radial,

[*]dmitrey.savelyev@yandex.ru   https://orcid.org/0000-0003-2282-3895

azimuthal polarization in the near zone of subwavelength ring gratings with a standard substrate and a GRIN substrate was studied in this paper. The height of individual zones of the element relief was varied. Numerical 3D-modeling was performed by the finite difference time domain (FDTD) method using the Meep software package [52].

1. The Gaussian beams diffraction on different substrates with varying relief height

The FDTD simulation was performed with the following simulation parameters: the wavelength λ of the input radiation was 0.532 μm, the spatial simulation step was $\lambda/30$, and the time step was $\lambda/(60c)$, where c is the speed of light.

The three-dimensional computational domain with 8.4 μm in size was considered in paper, which was surrounded on all sides by a 0.6 μm thick PML absorbing layer.

The effect of three different types of substrates was analyzes in the paper: a standard substrate with a refractive index of n = 1.47, and two types of GRIN substrates with different directions of refractive index change. The case when the refractive index changes from a maximum value in the center to a minimum value at the edges will be called a direct GRIN substrate, the opposite case, when the minimum refractive index is in the center and its uniform increase occurs toward the edges of the substrate, will be called a reverse GRIN substrate.

The minimum refractive index size in the case of GRIN substrates was n = 1.47 (similar to the standard substrate), the maximum refractive index was 2.7. The refractive index change step was 0.123. It should be noted that the GRIN substrates were rings of the same width with different radii, uniformly inscribed into each other on a square substrate measuring $16.5\lambda \times 16.5\lambda \times \lambda$. The height of all substrates was fixed and was λ.

The propagation of Laguerre–Gauss modes in free space can be described by the expression (1) [53–55]:

$$GL_{nm}(r, \phi, z) = \left(\frac{\sqrt{2}r}{\sigma(z)} \right)^{|m|} \exp(ikz) \exp[-i(2n + |m| + 1)\eta(z)] \times$$

$$\times \exp\left[\frac{i\pi r^2}{\lambda R(z)} \right] \exp\left[-\frac{r^2}{\sigma^2(z)} \right] L_n^{|m|}\left(\frac{2r^2}{\sigma^2(z)} \right) \exp(im\phi), \tag{1}$$

where $r^2 = x^2 + y^2$, $\phi = arctg(y/x)$, $\eta = arctg(z/z_0)$, $R(z) = z(1 + z_0^2/z^2)$ — radius of curvature of the light field parabolic front, $\sigma(z) = \sigma_0\sqrt{1 + z^2/z_0^2}$ — the effective beam radius, $z_0 = \pi\sigma_0^2/\lambda$ — confocal parameter, $L_n^m(x)$ — generalized Laguerre polynomial.

The input beams were first-order optical vortices (Laguerre-Gaussian modes $(0, 1)$) and Gaussian beams with $\sigma = 1.5$ μm with circular, radial and azimuthal polarizations. It should be noted that the circular polarization, in which the sign of the circular polarization is opposite to the sign of the introduced vortex phase singularity, was considered in this paper. In this case the maximum intensity value is formed on the optical axis for the Laguerre–Gaussian modes $(0, 1)$ [21].

The optical elements were considered: a diffraction axicon with a height of h = 1.06λ (the relief height was chosen based on the phase jump of π radians), a direct ring grating (the height of the relief rings changed from a maximum in the center hmax = 4.79λ to a minimum at the edge hmin = 1.06λ with a step of 0.53λ), and an inverse ring grating (similar maximum height and step of its change), in the case of which the height changed from a minimum in the center hmin = 1.06λ to a maximum value hmax = 4.79λ at the edge of the element. The period of all

optical elements considered was 1.05λ.

The longitudinal and transverse dimensions of the light segments obtained on the optical axis were estimated in the paper. The focal spot size was estimated by the standard full width at half maximum (FWHM) at the point of maximum intensity on the optical axis outside the element, and the length of the light needle along the radiation propagation axis (depth of focus – DOF) was estimated in a similar manner.

It should be noted that a direct GRIN substrate allows for additional focusing of radiation and, accordingly, a smaller focal spot size, while in the case of a reverse GRIN substrate, which in this case acts as a diffusing lens, an extension of the light segment size is observed.

Fig. 1 shows the passage of a Gaussian beam through a diffraction axicon with a standard
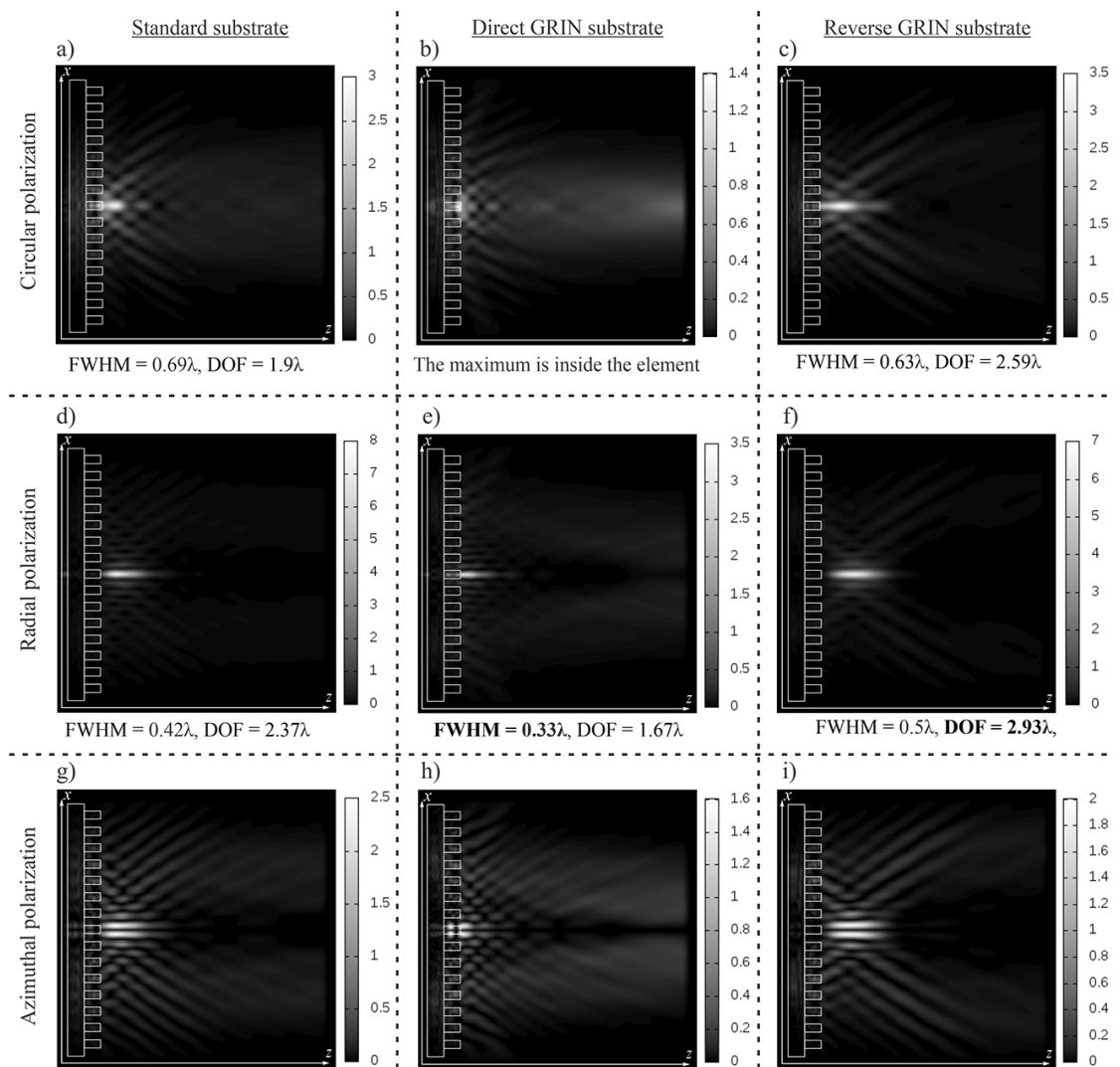

Fig. 1. Longitudinal cross-section (xz) of Gaussian beam propagation (intensity), diffraction axicon for different types of substrate, circular polarization (a, b, c), radial polarization (d, e, f), azimuthal polarization (g, h, i)

substrate and GRIN substrates for different polarizations of laser radiation; the element relief

height was h = 1.06λ, and the numerical aperture was NA = 0.95. Focusing on the optical axis is observed for circular and radial polarizations of laser radiation.

The minimum focal spot size was obtained for radial polarization with a direct GRIN substrate FWHM = 0.33λ, which is 21.4% smaller than the focal spot size obtained with the same type of polarization for a standard substrate.

The maximum size of the light needle was also obtained for radial polarization, but for a reverse GRIN substrate DOF = 2.93λ, which is 23.6% longer than the light needle obtained in the case of a standard substrate. It also should be noted that for circular polarization, the use of a direct GRIN substrate led to focusing of the beam inside the element.

Let us now consider the diffraction of Gaussian beams on the direct and inverse ring gratings described above (Fig. 2 and Fig. 3, respectively). We will also monitor the longitudinal and transverse sizes of the light segment on the optical axis. Accordingly, we will now consider circular and radial polarization of laser radiation.
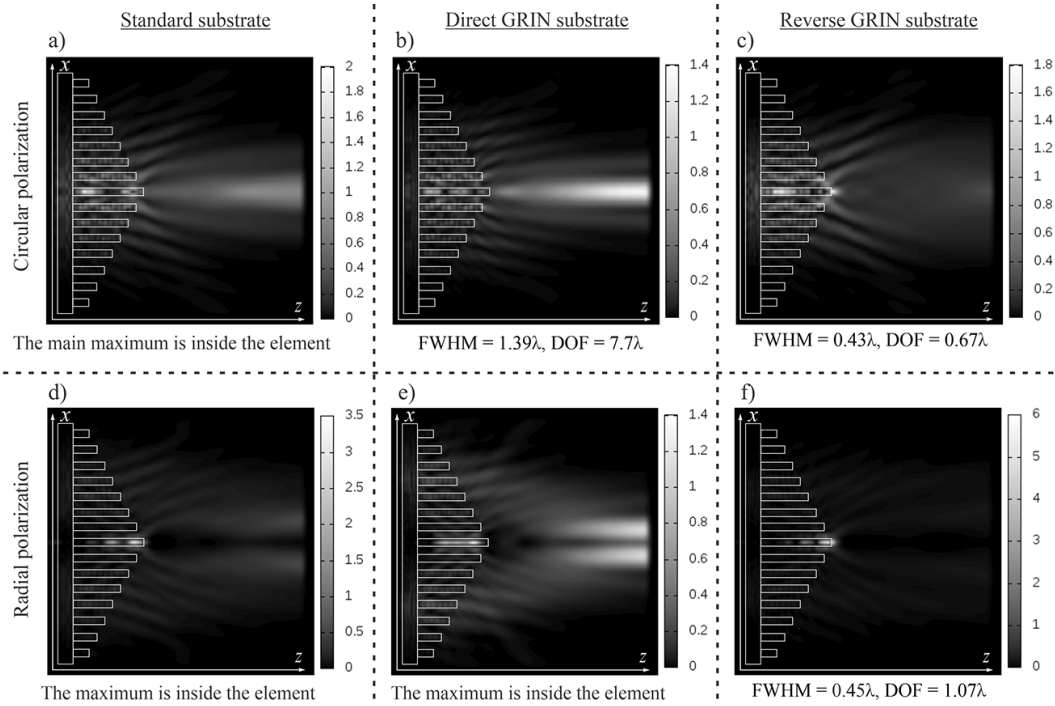

Fig. 2. Longitudinal cross-section (xz) of Gaussian beam propagation (intensity), direct ring grating for different types of substrate, circular polarization (a, b, c), radial polarization (d, e, f)

So, as can be seen from Fig. 2, the formation of intensity peaks on the optical axis inside the element is observed for the standard substrate, as well as for the direct GRIN substrate with radial polarization. The smallest focal spot size was obtained for the reverse GRIN substrate with circular polarization FWHM = 0.43λ. The maximum size of the light needle was also obtained for circular polarization with the direct GRIN substrate (DOF = 7.7λ).

It should be noted that in the case of the direct GRIN substrate for radial polarization a redistribution of intensity from the optical axis and the formation of a ring are observed at a distance of over 4λ from the element relief.

In the case of the inverse ring grating (Fig. 3) the main intensity peak is formed inside

the element for circular polarization and the standard and direct GRIN substrates, but then the formation of maxima of comparable intensity values was observed outside the element. The minimum focal spot size was obtained for the direct GRIN substrate with radial polarization (FWHM $= 0.54\lambda$). In this case, the maximum size of the light needle also was obtained: DOF $= 8.2\lambda$.

The main maximum inside, outside:
FWHM$_1 = 0.6\lambda$, DOF$_1 = 1.6\lambda$,
FWHM$_2 = 0.73\lambda$, DOF$_2 = 2.02\lambda$

The main maximum inside, outside:
FWHM $= 0.59\lambda$, DOF $= 1.65\lambda$

FWHM$_1 = 0.6\lambda$, DOF$_1 = 1.73\lambda$,
FWHM$_2 = 0.71\lambda$, DOF$_2 = 3.74\lambda$

FWHM $= 0.87\lambda$, DOF $= 4.45\lambda$

FWHM $= 0.54\lambda$, DOF $= 8.2\lambda$

FWHM$_1 = 0.55\lambda$, DOF$_1 = 1.1\lambda$,
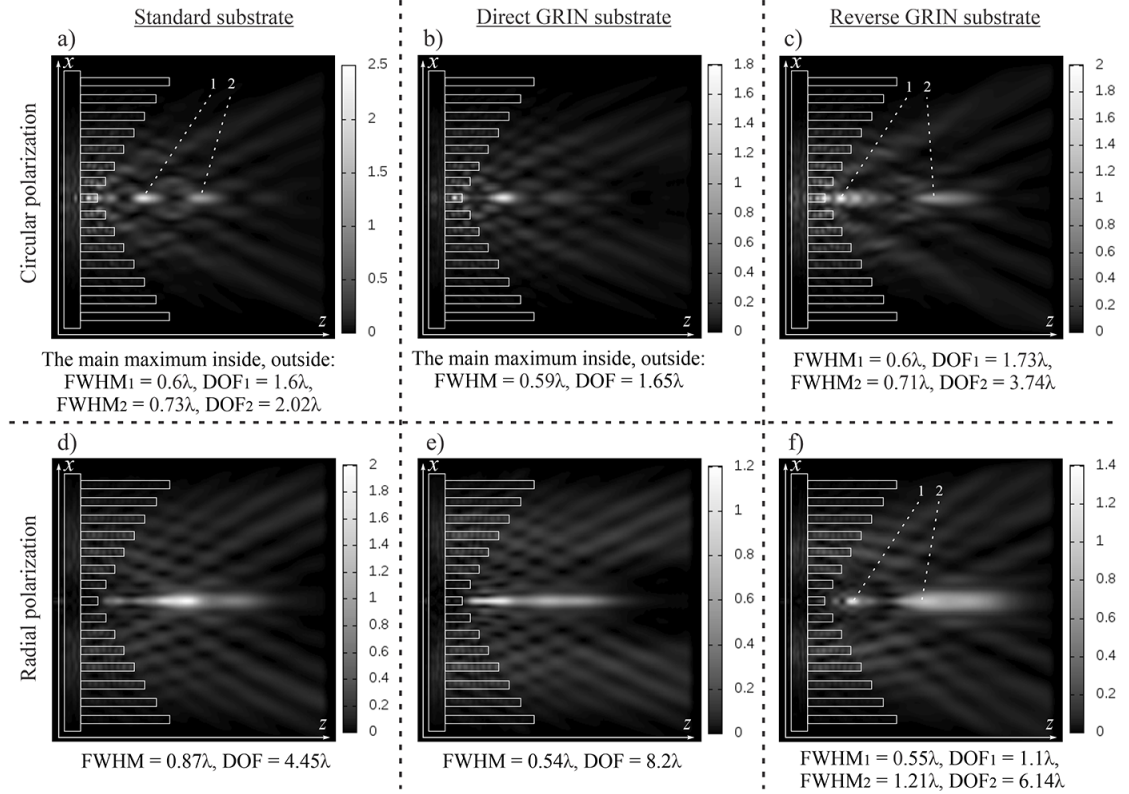FWHM$_2 = 1.21\lambda$, DOF$_2 = 6.14\lambda$

Fig. 3. Longitudinal cross-section (xz) of Gaussian beam propagation (intensity), inverse ring grating for different types of substrate, circular polarization (a, b, c), radial polarization (d, e, f)

Thus, the direct GRIN substrate with radial polarization of laser radiation demonstrated its efficiency for Gaussian beams: the minimum focal spot size (FWHM $= 0.33\lambda$) was obtained for the usual relief of the diffraction axicon, the maximum size of the light needle was obtained for the relief of the inverse ring grating (DOF $= 8.2\lambda$).

Let us further consider similar optical elements with a different type of input laser radiation — the Laguerre–Gauss mode $(0, 1)$.

2.   The Laguerre-Gauss mode $(0, 1)$ diffraction on different substrates with varying relief height

This section presents studies on the influence of changes in the height of individual relief zones, the type of substrates, and the polarization of the input laser radiation for Laguerre–Gaussian modes $(0, 1)$ on the diffraction pattern in the near zone.

Fig. 4 shows the passage of first-order optical vortices through a standard substrate and GRIN substrates for different laser radiation polarizations (the element relief height was h $= 1.06\lambda$). The

focusing on the optical axis is observed for circular and azimuthal laser radiation polarizations as expected [21].

The minimum focal spot size was obtained for the direct GRIN substrate for azimuthal polarization of laser radiation (FWHM = 0.42λ). However, it should be noted that the decrease in the focal spot size is insignificant. The maximum size of the light needle was also obtained for azimuthal polarization in the case of the reverse GRIN substrate (DOF = 3.07λ).
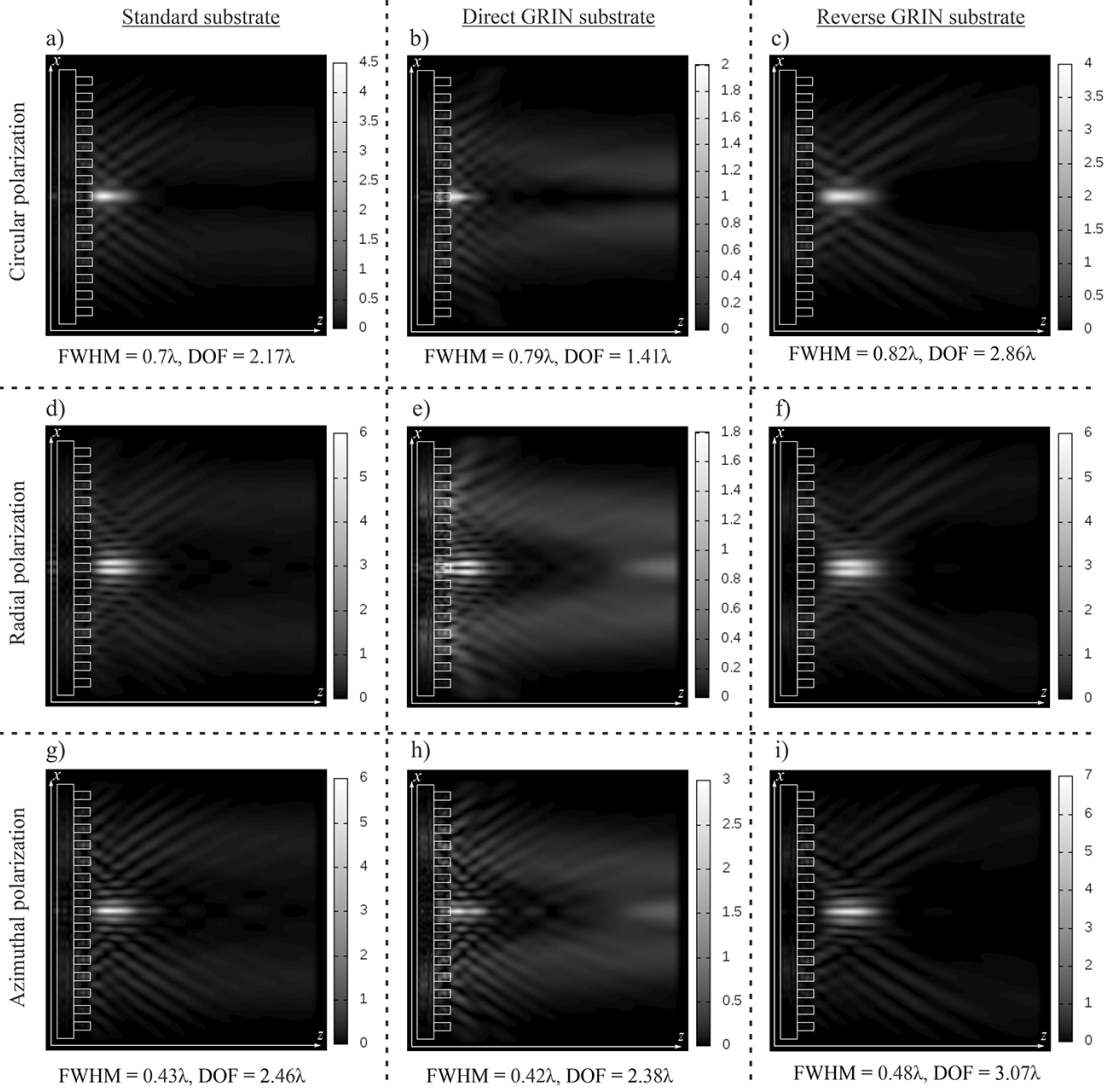

Fig. 4. Longitudinal cross-section (xz) of the propagation of first-order optical vortices (intensity), diffraction axicon for different types of substrate, circular polarization (a, b, c), radial polarization (d, e, f), azimuthal polarization (g, h, i)

Let us consider further, as before, the direct and inverse ring gratings (Fig. 5 and 6, respectively), with circular and azimuthal polarization of laser radiation.

As can be seen from Fig. 5, the focusing is observed inside the element for a standard substrate, as in the case of a Gaussian beam. It should be noted that the focusing on the optical axis is

observed for a direct ring substrate only in two cases: for a reverse GRIN substrate with circular polarization (with a focal spot size of FWHM = 0.52 λ) and for a direct GRIN substrate in the case of azimuthal polarization (DOF = 4.91λ).
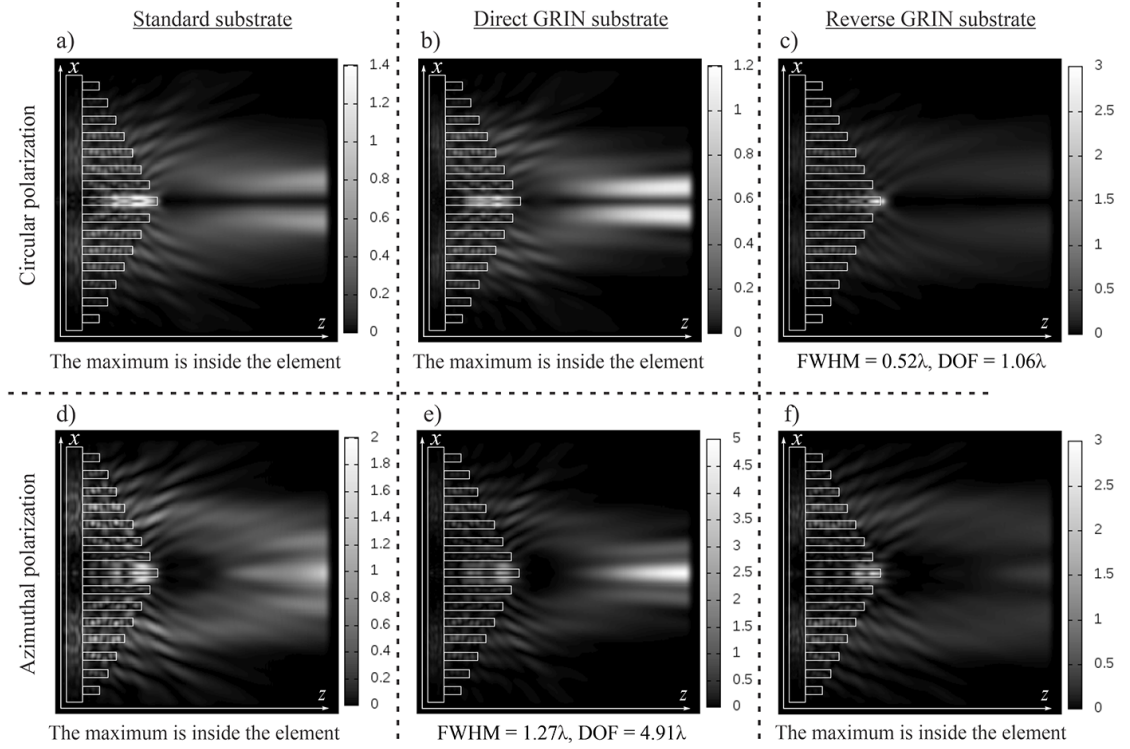

Fig. 5. Longitudinal cross-section (xz) of the propagation of first-order optical vortices (intensity), direct ring grating for different types of substrate, circular polarization (a, b, c), azimuthal polarization (d, e, f)

For a direct GRIN substrate a ring is formed in the case of circular polarization. But a light needle was formed on the optical axis for a similar type of element and polarization for a Gaussian beam.

In the case of a reverse ring grating (Fig. 6), for the considered types of polarization, intensity oscillations are observed on the optical axis. Moreover, for circular polarization, with distance from the element, a redistribution of intensity from the optical axis is observed and intensity ring with a minimum intensity value on the optical axis is formed.

The minimum focal spot size was obtained for a direct GRIN substrate with azimuthal polarization of laser radiation (FWHM = 0.43λ) in the first maximum outside the element.

The maximum size of the light needle is also obtained for this case, i.e. in the case of the reverse GRIN substrate (DOF = 5.99λ). However, it should also be noted that a powerful light needle is formed for the case of the reverse GRIN substrate with azimuthal polarization (DOF = 5.58λ).

Thus, the use of both the direct and reverse GRIN substrates also allows one to obtain longer focal segments for the Laguerre-Gaussian modes $(0, 1)$ than when using a standard substrate.

In particular, the use of the reverse GRIN substrate for circular polarization allowed one to achieve an increase in the focal light segment size by 31.8% (DOF = 2.86λ) than when using a

standard substrate in the case of a diffractive axicon. And both the direct and reverse GRIN substrates in the case of a reverse ring grating for azimuthal polarization allow one to obtain an extended light segment.

Moreover, the formation of a light needle 2.43 times longer than the light needle formed by a standard diffractive axicon (DOF = 5.99λ) is observed in the case of the direct GRIN substrate.

It should be noted that for a Gaussian beam, the maximum light tip size was also obtained for the inverse ring grating relief (DOF = 8.2λ) and the direct GRIN substrate.
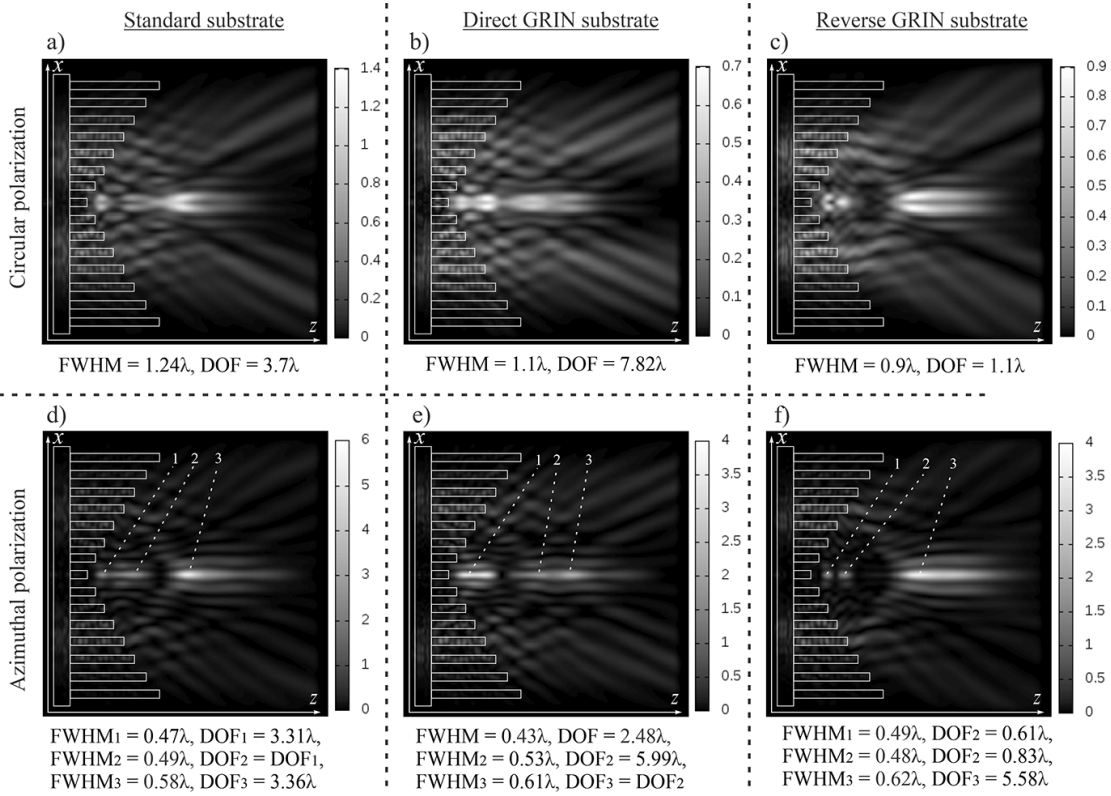

Fig. 6. Longitudinal cross-section (xz) of the propagation of first-order optical vortices (intensity), inverse ring grating for different types of substrate, circular polarization (a, b, c), azimuthal polarization (d, e, f)

Conclusion

The FDTD method was used to simulate the diffraction of Gaussian beams and Laguerre-Gauss modes $(0, 1)$ with circular, radial, azimuthal polarization on subwavelength ring gratings with standard and GRIN substrates in this paper. The height of individual zones of the element relief was varied.

It should be noted that the use of a direct GRIN substrate resulted in a decrease in the focal spot size for both the Gaussian beam (FWHM = 0.33λ) and the Laguerre–Gaussian mode $(0, 1)$, FWHM = 0.42λ, compared to the action of a diffractive axicon with a conventional substrate.

The influence of the direct GRIN substrate for individual cases also manifested itself in the formation of long light segments. In particular, for Gaussian beams, the maximum size of the

light needle was obtained for the relief of the inverse ring grating (DOF = 8.2λ) with radial polarization. In the case of an optical vortex, this type of element also made it possible to form an extended light segment with azimuthal polarization (DOF = 5.99λ).

The use of the inverse GRIN substrate also resulted in the formation of extended light segments, in particular, for the inverse ring grating in the case of the Laguerre-Gaussian mode $(0, 1)$, a powerful light needle with DOF = 5.58λ was obtained. The same type of element, when illuminated by a conventional Gaussian beam, allowed the formation of a focal light segment with an extension of DOF = 6.14λ.

References

[1] Y.Kang, J.Wang, Y.Zhao, X.Zhao, H.Tao, Y.Xu, High refractive index GRIN lens for IR optics, *Materials*, **16**(2023), no. 7, 2566. DOI: 10.3390/ma16072566.

[2] K.A.Richardson et al., Advances in infrared gradient refractive index (GRIN) materials: a review, *Optical Engineering*, **59**(2020), no. 11, 112602. DOI: 10.1117/1.OE.59.11.112602.

[3] Z.Zhang et al., Refractive index measurement deflectometry for measuring gradient refractive index lens, *Optics Express*, **32**(2024), no. 7, 12620–12635. DOI: 10.1364/OE.518670.

[4] D.H.Lippman et al., Freeform gradient-index media: a new frontier in freeform optics, *Optics Express*, **29**(2021), no. 22, 36997–37012. DOI: 10.1364/OE.443427.

[5] J.M.Luque-Gonzalez et al., An ultracompact GRIN-lens-based spot size converter using subwavelength grating metamaterials, *Laser & Photonics Reviews*, **13**(2019), no. 11, 1900172. DOI: 10.1002/lpor.201900172.

[6] C.Guo, T.Urner, S.Jia, 3D light-field endoscopic imaging using a GRIN lens array, *Applied Physics Letters*, **116**(2020), no. 10, 101105. DOI: 10.1063/1.5143113.

[7] G.I.Greisukh, I.Y.Levin, E.G.Ezhov, Ultra-high-aperture infrared triplet with a GRIN lens: modeling stages of composite gradient-index material and potential possibilities of the optical system, *Journal of Optical Technology*, **91**(2024), no. 3, 137–141.
DOI: 10.1364/JOT.91.000137.

[8] P.Lalanne, P.Chavel, Metalenses at visible wavelengths: past, present, perspectives, *Laser & Photonics Reviews*, **11**(2017), no. 3, 1600295. DOI: 10.1002/lpor.201600295.

[9] J.E.Gomez-Correa et al., Symmetric gradient-index media reconstruction, *Optics Express*, **31**(2023), no. 18, 29196–29212. DOI: 10.1364/OE.498649.

[10] J.E.Gomez-Correa, Geometrical-light-propagation in non-normalized symmetric gradient-index media, *Optics Express*, **30**(2022), no. 19, 33896–33910. DOI: 10.1364/OE.465957.

[11] L.Wei, G.Li, M.Song, C.H.Wang, W.Zhang, Determination of gradient index based on laser beam deflection by stochastic particle swarm optimization, *Applied Physics B*, **127**(2021), no. 9, 131. DOI: 10.1007/s00340-021-07676-9.

[12] Y.F.Chien et al., Dual GRIN lens two-photon endoscopy for high-speed volumetric and deep brain imaging, *Biomedical Optics Express*, **12**(2021), no. 1, 162–172. DOI: 10.1364/BOE.405738.

[13] G.M.Williams, J. Paul Harmon, Dispersion controlled nanocomposite gradient index lenses, *Optics Continuum*, **2**(2023), no. 2, 456–472. DOI: 10.1364/OPTCON.481205.

[14] D.A.Savelyev, A.V.Ustinov, S.N.Khonina, N.L.Kazanskiy, Layered lens with a linear dependence of the refractive index change, *Proceedings of SPIE*, **9807**(2016), 203–209. DOI: 10.1117/12.2234404.

[15] A.K.Baghel, S.S.Kulkarni, S.K.Nayak, Far-field wireless power transfer using GRIN lens metamaterial at GHz frequency, *IEEE Microwave and Wireless Components Letters*, **29**(2019), no. 6, 424–426. DOI: 10.1109/LMWC.2019.2912056.

[16] D.A.Savelyev, S.V.Karpeev, Development of 3D Microstructures for the Formation of a Set of Optical Traps on the Optical Axis, *Photonics*, **10**(2023), no. 2, 117. DOI: 10.3390/photonics10020117.

[17] H.Ohno, Symplectic ray tracing based on Hamiltonian optics in gradient-index media, *JOSA A*, **37**(2020), no. 3, 411–416. DOI: 10.1364/JOSAA.378829.

[18] H.Ohno, T.Usui, Neural network gradient-index mapping, *OSA Continuum*, **4**(2021), no. 10, 2543–2551. DOI: 10.1364/OSAC.437395.

[19] R.Azizkhani, D.Hebri, S.Rasouli, Gaussian beam diffraction from radial structures: detailed study on the diffraction from sinusoidal amplitude radial gratings, *Optics Express*, **31**(2023), no. 13, 20665–20682. DOI: 10.1364/OE.489659.

[20] A.P.Porfirev et al., Phase singularities and optical vortices in photonics, *Phys. Usp.*, **192**(2022), no. 8, 841–866. DOI: 10.3367/UFNe.2021.07.039028.

[21] D.Savelyev, N.Kazanskiy, Near-Field Vortex Beams Diffraction on Surface Micro-Defects and Diffractive Axicons for Polarization State Recognition, *Sensors*, **21**(2021), no. 6, 1973. DOI: 10.3390/s21061973.

[22] S.N.Khonina, S.V.Karpeev, M.A.Butt, Spatial-light-modulator-based multichannel data transmission by vortex beams of various orders, *Sensors*, **21**(2021), no. 9, 2988. DOI: 10.3390/s21092988.

[23] Y.Lian et al., OAM beam generation in space and its applications: A review, *Optics and Lasers in Engineering*, **151**(2022), 106923. DOI: 10.1016/j.optlaseng.2021.106923.

[24] D.A.Savelyev, Features of a Gaussian beam near-field diffraction upon variations in the relief height of subwavelength silicon optical elements, *Computer Optics*, **47**(2023), no. 6, 938–947 (in Russian). DOI: 10.18287/2412-6179-CO-1402.

[25] V.V.Kotlyar et al., Spin–Orbital Transformation in a Tight Focus of an Optical Vortex with Circular Polarization, *Applied Sciences*, **13**(2023), no. 14, 8361. DOI: 10.3390/app13148361.

[26] S.N.Khonina, A.V.Ustinov, S.G.Volotovskiy, N.A.Ivliev, V.V.Podlipnov, Influence of optical forces induced by paraxial vortex Gaussian beams on the formation of a microrelief on carbazole-containing azopolymer films, *Applied Optics*, **59**(2020), no. 29, 9185-9194. DOI: 10.1364/AO.398620.

[27] J.Baltrukonis, O.Ulcinas, S.Orlov, V.Jukna, High-order vector bessel-gauss beams for laser micromachining of transparent materials, *Physical Review Applied*, **16**(2021), no. 3, 034001. DOI: 10.1103/PhysRevApplied.16.034001.

[28] B.Wang et al., Generating optical vortex beams by momentum-space polarization vortices centred at bound states in the continuum, *Nature Photonics*, **14**(2020), no. 10, 623–628. DOI: 10.1038/s41566-020-0658-1.

[29] A.Brimis, K.G.Makris, D.G.Papazoglou, Optical vortices shape optical tornados, *Optics Express*, **31**(2023), no. 17, 27582–27593. DOI: 10.1364/OE.495836.

[30] D.A.Savelyev, The investigation of the features of focusing vortex super-Gaussian beams with a variable-height diffractive axicon, *Computer Optics*, **45**(2021), no. 2, 214–221 (in Russian). DOI: 10.18287/2412-6179-CO-862.

[31] J.Adams, I.Agha, A.Chong, Spatiotemporal optical vortex reconnections of multi-vortices, *Scientific Reports*, **14**(2024), no. 1, 5483. DOI: 10.1038/s41598-024-54216-4.

[32] D.Savelyev, S.Degtyarev, Features of the Optical Vortices Diffraction on Silicon Ring Gratings, *Optical Memory and Neural Networks*, **31**(2022), no. 1, 55–66. DOI: 10.3103/S1060992X22050095.

[33] K.Zhang, Y.Wang, Y.Yuan, S.N.Burokur, A review of orbital angular momentum vortex beams generation: from traditional methods to metasurfaces, *Applied Sciences*, **10**(2020), no. 3, 1015. DOI: 10.3390/app10031015.

[34] D.A.Savelyev, Peculiarities of focusing circularly and radially polarized super-Gaussian beams using ring gratings with varying relief height, *Computer Optics*, **46**(2022), no. 4, 537–546 (Russian). DOI: 10.18287/2412-6179-CO-1131.

[35] M.Dong, C.Zhao, Y.Cai, Y.Yang, Partially coherent vortex beams: Fundamentals and applications, *Science China Physics, Mechanics & Astronomy*, **64**(2021), no. 2, 224201. DOI: 10.1007/s11433-020-1579-9.

[36] D.L.Andrews, Symmetry and quantum features in optical vortices, *Symmetry*, **13**(2021), no. 8, 1368. DOI: 10.3390/sym13081368.

[37] N.Jimenez, V.Romero-Garcia, L.M.Garcia-Raffi, F.Camarena, K.Staliunas, Sharp acoustic vortex focusing by Fresnel-spiral zone plates, *Applied Physics Letters*, **112**(2018), no. 20, 204101. DOI: 10.1063/1.5029424.

[38] E.V.Barshak et al., Robust higher-order optical vortices for information transmission in twisted anisotropic optical fibers, *Journal of Optics*, **23**(2021), no. 3, 035603. DOI: 10.1088/2040-8986/abda85.

[39] Y.Shen et al., Optical vortices 30 years on: OAM manipulation from topological charge to multiple singularities, *Light: Science & Applications*, **8**(2019), no. 1, 1–29. DOI: 10.1038/s41377-019-0194-2.

[40] D.A.Savelyev, The Features of the Optical Traps Formation Using Silicon Ring Gratings with Variable Height, *Photonics*, **10**(2023), no. 11, 1264. DOI: 10.3390/photonics10111264.

[41] J.Bayat, F.Hajizadeh, A.M. Khazaei, S.Rasouli, Gear-like rotatable optical trapping with radial carpet beams, *Sci. Rep.*, **10**(2020), no. 1, 11721. DOI: 10.1038/s41598-020-68695-8.

[42] A.A.Sirenko et al., Terahertz vortex beam as a spec-troscopic probe of magnetic excitations, *Physical Review Letters*, **122**(2019), no. 23, 237401. DOI: 10.1103/PhysRevLett.122.237401.

[43] S.N.Khonina, M.A.Butt, N.L.Kazanskiy, A Review on Reconfigurable Metalenses Revolutionizing Flat Optics, *Adv. Optical Mater*, **12**(2024), no. 4, 2302794. DOI: 10.1002/adom.202302794.

[44] S.Lightman, G.Hurvitz, R.Gvishi, A.Arie, Miniature wide-spectrum mode sorter for vortex beams produced by 3D laser printing, *Optica*, **4**(2017), no. 6, 605–610. DOI: 10.1364/OPTICA.4.000605.

[45] S.Yu, Potentials and challenges of using orbital angular momentum communications in optical interconnects, *Optics Express*, **23**(2015), no. 3, 3075–3087. DOI: 10.1364/OE.23.003075.

[46] S.N.Khonina, N.L.Kazanskiy, P.A.Khorin, M.A.Butt, Modern types of axicons: new functions and applications, *Sensors*, **21**(2021), no. 19, 6690. DOI: 10.3390/s21196690.

[47] Z.Yang et al., Design of bottle beam based on dual-beam for trapping particles in air, *Applied Optics*, **58**(2019), no. 10, 2471. DOI: 10.1364/AO.58.002471.

[48] D.A.Savelyev, S.N.Khonina, Characteristics of sharp focusing of vortex Laguerre-Gaussian beams, *Computer Optics*, **39**(2015), no. 5, 654–662 (in Russian). DOI: 10.18287/0134-2452-2015-39-5-654-662.

[49] C.Shi et al., Sub-wavelength longitudinally polarized optical needle arrays generated with tightly focused radially polarized Gaussian beam, *Optics Communications*, **505**(2022), 127506. DOI: 10.1016/j.optcom.2021.127506.

[50] D.A.Savelyev, The Comparison of Laser Radiation Focusing by Diffractive Axicons and Annular Gratings with Variable Height Using High-performance Computer Systems, Proceedings of IEEE – 2021 Photonics & Electromagnetics Research Symposium (PIERS), 2021, 2709–2716. DOI: 10.1109/PIERS53385.2021.9694860.

[51] N.L.Kazanskiy, S.N.Khonina, Nonparaxial effects in lensacon optical systems, *Optoelectronics, Instrumentation and Data Processing*, **53**(2017), no. 5, 484–493. DOI: 10.3103/S8756699017050089.

[52] M.Rani, J.Kashyap, U.Singh, A.Kapoor, Optimisation of dielectric spacer layer thickness in Ag nanospheres/ITO/c-Si structure for plasmonic solar cells using FDTD simulation, *Materials Technology*, **37**(2022), no. 10, 1320–1328. DOI: 10.1080/10667857.2021.1940046.

[53] M.S.Soskin, M.V.Vasnetsov, Singular optics, *Progress in optics*, **42**(2001), 219–276. DOI: 10.1016/S0079-6638(01)80018-4.

[54] A.V.Chernykh, N.V.Petrov, Optical vortex trajectory of the edge-diffracted single-charged Laguerre-Gaussian beam, *Optics and Lasers in Engineering*, **139**(2021), 106504. DOI: 10.1016/j.optlaseng.2020.106504.

[55] V.A.Soifer et al., Computer Design of Diffractive Optics, *Woodhead Publishing Series in Electronic and Optical Materials*, **50**(2013). DOI: 10.1533/9780857093745.

Исследование дифракции гауссовых пучков и оптических вихрей в ближней зоне субволновых оптических элементов переменной высоты

Дмитрий А. Савельев
Самарский национальный исследовательский университет
Самара, Российская Федерация

Аннотация. В работе методом конечных разностей во временной области было проведено моделирование распространения гауссовых пучков и оптических вихрей первого порядка с круговой, радиальной, азимутальной поляризацией на субволновых кольцевых решетках со стандартной и GRIN-подложками. Изменялась высота отдельных зон оптических элементов. Показано, что можно подобрать тип пучка и параметры элемента таким образом, чтобы на оптической оси формировалась длинная световая игла (до 8.2λ), а также узкое фокальное пятно (до 0.33λ).

Ключевые слова: гауссовы пучки, оптические вихри, FDTD, GRIN, субволновые кольцевые решетки, Meep.